

Discovery of 9 Ly α emitters at redshift $z \sim 3.1$ using narrow-band imaging and VLT spectroscopy¹

R.-P. Kudritzki^{2,3} and R. H. Méndez

Munich University Observatory, Scheinerstr. 1, 81679 Munich, Germany

kudritzki@usm.uni-muenchen.de, mendez@usm.uni-muenchen.de

J. J. Feldmeier and R. Ciardullo

Dept. of Astron. and Astrophys., Penn State Univ., 525 Davey Lab, Univ. Park, PA 16802

G. H. Jacoby

Kitt Peak National Observatory, P.O.Box 26732, Tucson, AZ 85726

K. C. Freeman

Mt. Stromlo and Siding Spring Observatories, Weston Creek P.O., ACT 2611, Australia

M. Arnaboldi and M. Capaccioli

Osservatorio Astronomico di Capodimonte, V. Moiariello 16, Napoli 80131, Italy

O. Gerhard

Astronomisches Institut, Universität Basel, CH-4102 Binningen, Switzerland

and

H. C. Ford

Phys. and Astron. Dept., John Hopkins Univ., Homewood Campus, Baltimore, MD 21218

ABSTRACT

Narrow-band imaging surveys aimed at detecting the faint emission from the 5007 Å [O III] line of intracluster planetary nebulae in Virgo also probe high redshift $z \sim 3.1$ Ly α emitters. Here we report on the spectroscopic identification of 9 Ly α emitters at $z = 3.13$ with fluxes between 2×10^{-17} and 2×10^{-16} erg cm $^{-2}$ s $^{-1}$ obtained with the FORS spectrograph at Unit 1 of the ESO Very Large Telescope (VLT UT1).

²Max-Planck-Institut für Astrophysik, Karl-Schwarzschild-Str. 1, 85740 Garching, Germany

³Steward Observatory, Univ. of Arizona, 933 N. Cherry Av., Tucson, AZ 85721

The spectra of these high redshift objects show a narrow, isolated Ly α emission with very faint (frequently undetected) continuum, indicating a large equivalent width. No other features are visible in our spectra. Our Ly α emitters are quite similar to those found by Hu (1998), Cowie & Hu (1998) and Hu et al. (1998). For a flat universe with $H_0=70 \text{ km s}^{-1} \text{ Mpc}^{-1}$ and $q_0=0.5$ ($\Omega_\Lambda=0$), the Ly α luminosity of the brightest source is $1.7 \times 10^9 \text{ L}_\odot$, and the comoving space density of the Ly α emitters in the searched volume is $5 \times 10^{-3} \text{ Mpc}^{-3}$.

Using simple population synthesis models, on the assumption that these sources are regions of star formation, we conclude that the nebulae are nearly optically thick and must have a very low dust content, in order to explain the high observed Ly α equivalent widths. For the cosmological and star formation parameters we adopted, the total stellar mass produced would seem to correspond to the formation of rather small galaxies, some of which are perhaps destined to merge. However, one of our sources might become a serious candidate for a proto-giant spheroidal galaxy if we assumed continuous star formation, a low mass cutoff of 0.1 M_\odot in the IMF, and a flat accelerating universe with $\Omega_0=0.2$ and $\Omega_\Lambda=0.8$.

The implied star formation density in our sampled comoving volume is probably somewhat smaller than, but of the same order of magnitude as the star formation density at $z \sim 3$ derived by other authors from Lyman-break galaxy surveys. This result agrees with the expectation that the Ly α emitters are a low-metallicity (or low-dust) tail in a distribution of star forming regions at high redshifts. Finally, the Ly α emitters may contribute as many H-ionizing photons as QSOs at $z \sim 3$. They are therefore potentially significant for the ionization budget of the early universe.

Subject headings: cosmology: observations — early universe — galaxies: clusters: individual (Virgo cluster) — galaxies: intergalactic medium — galaxies: evolution — galaxies: formation

1. Introduction

Ly α emitting galaxies at high redshift are of much interest for studies of galaxy formation. While early surveys failed to find such objects (e.g. Thompson et al. 1995), recent narrow-band imaging searches with spectroscopic follow-up identified a number of Ly α emitters at high z , first in fields near high-redshift QSOs (Hu & McMahon 1996) and later in blank fields (Cowie & Hu 1998; Hu et al. 1998; Pascale et al. 1998). These Ly α emitters have typically very faint continua and

¹Based on observations collected at the European Southern Observatory, Cerro Paranal, Chile; ESO programmes 63.N-0530 and 63.I-0007

high Ly α equivalent widths, i.e., may represent an early phase of galaxy formation when substantial amounts of dust had not yet formed.

Here we report on the discovery of 9 Ly α emitters at redshift $z = 3.1$ during our program of studying the intracluster planetary nebula (PN) population in the Virgo cluster, which uses similar narrow-band imaging techniques to identify candidate PNs. The first indication of the existence of a diffuse intracluster stellar population in Virgo was the discovery by Arnaboldi et al. (1996) that a few PNs in the galaxy NGC 4406 (M 86; redshift -230 km s^{-1}) have redshifts typical of the Virgo cluster (around $+1300 \text{ km s}^{-1}$). Subsequently, direct evidence for red giant stars belonging to this stellar population was reported by Ferguson et al. (1998). Because PNs offer the chance to measure radial velocities and perhaps even abundances for such a diffuse population, a search for intracluster PNs in different positions across the Virgo cluster started immediately and produced several dozens of PN candidates (Méndez et al. 1997, Feldmeier et al. 1998) in a total surveyed area of 0.23 deg^2 .

The “on-band/off-band” narrow-band filter technique used to discover the PN candidates (see e.g. Jacoby et al. 1992) allows the detection of a single emission line. This is not necessarily the desired [O III] $\lambda 5007$; it might be another emission line at higher z , redshifted into the on-band filter. For example [O II] $\lambda 3727$ at $z = 0.35$, or Ly α at $z = 3.13$. In previous work (Méndez et al. 1997) we argued that most of our detections had to be real PNs because (a) the surface density of emission line galaxies derived from earlier studies was not high enough to explain all the detections; (b) the luminosity function of the detected sources is in good agreement with the PN luminosity functions derived in several Virgo galaxies (Jacoby et al. 1990).

We have used the first ESO Very Large Telescope (VLT) unit (UT1) with the Focal Reducer and Spectrograph (FORS) in multi-object spectroscopic mode, and the 4-m Anglo-Australian Telescope (AAT) with the 2-degree-field (2df) fiber spectrograph. Our purpose was to confirm the nature of the Virgo intracluster PN candidates, to measure their radial velocities, and (in the VLT case) to detect the faint diagnostic lines required for abundance determinations.

The present paper reports on the results of the VLT+FORS observations. The AAT+2df observations, which confirm the existence of Virgo intracluster PNs through the detection of both the $\lambda 4959$ and $\lambda 5007$ [O III] lines (Freeman et al. 1999), will be presented and discussed by Freeman et al. (2000, in preparation).

2. Observations and first results

For the purpose of detecting faint nebular diagnostic lines with VLT+FORS (ESO programme 63.N-0530), we selected Field 1 of Feldmeier et al. (1998) as our first priority, because it had the brightest PN candidates, with a luminosity function cutoff about half a magnitude brighter ($m_{5007} = 25.8$) than elsewhere in the Virgo cluster (see Feldmeier et al. 1998). The total area of Field 1 is 256 arcmin^2 . We also wanted to use FORS (ESO programme 63.I-0007) to verify

the PN nature of candidates in the smaller “La Palma Field” (50 arcmin^2 , Méndez et al. 1997), with magnitudes m_{5007} between 26.8 and 28.6. The lack of bright PNs in the La Palma Field was understandable in Méndez et al. (1997) as a consequence of the sample size effect: if the total PN sample is small, the chance of finding a bright PN is too small.

The observations were made with FORS at the VLT UT1 on the nights of 11/12, 15/16, 16/17 and 19/20 April 1999. Since the FORS field is slightly smaller than $7 \times 7 \text{ arc mins}$ (with the standard collimator), we selected a portion of Field 1 where several of the brightest candidates were located, and took on-band and off-band images of the selected portion of Field 1, and of the La Palma Field, on the night 11/12, using FORS in imaging mode.

The on-band and off-band interference filters we used have, respectively, central wavelengths 5039 and 5300 Å, and FWHMs 52 and 250 Å. Some 50 stellar images in the short on-band and off-band FORS exposures (10 min and 3 min, respectively) were used together with the corresponding stellar images in the Kitt Peak and La Palma discovery images to define coordinate transformations that gave the pixel values of the positions of the PN candidates in the FORS images, given the pixel values of their positions in the discovery images. In this way it was possible to define the FORS slit positions with sufficient accuracy (in fact, the brightest PN candidates were visible in the short on-band FORS exposures, allowing us to verify directly the accuracy of the pixel transformation, with typical errors below 0.5 pixels, which is equivalent to 0.1 arc sec).

On the night of 15/16 April, R.P.K. and R.H.M. started FORS multi-object spectroscopy (MOS) in Field 1, using grism 300V without any order separation filter, for maximum spectral coverage. This grism gives a spectral resolution of about 10 Å, at 5000 Å, for slitlets 1 arc sec wide. Of the 19 available slitlets, 10 were placed at the positions of PN candidates (numbers 1, 4, 5, 6, 16, 17, 21, 26, 27, 42, ordered by brightness as measured by Feldmeier). These candidates had magnitudes m_{5007} between 25.8 and 26.4. The remaining 9 slitlets were placed on stars or galaxies in the field, in order to check the slitlet positioning (which was done by taking a short exposure without grism through the slitlets) and to help locate the dispersion lines as a function of position across the field, which is important in the case of spectra consisting of isolated emission lines.

After taking 5 exposures of 40 min each in Field 1, all with the same slitlet configuration, and having made preliminary on-line reductions, it was clear that the [O III] emission line candidates were not PNs. Object 1 showed one strong isolated emission line at 5021 Å. It cannot be [O III] $\lambda 5007$ because there is no hint of the companion line $\lambda 4959$ at the corresponding wavelength. Object 5 was identified as a starburst with $z = 0.35$; it shows narrow emission lines with a continuum, $\lambda 3727$ is redshifted into the on-band filter, and H β and the [O III] lines 4959 and 5007 are visible, also redshifted with $z = 0.35$. Object 17 was not detected. The remaining 7 objects were identified as continuum objects. Many of them are galaxies: they show redshifted emissions.

In summary, none of the candidates tested in Field 1 with VLT+FORS are PNs. This result in fact solves a problem, because these Field 1 candidates were surprisingly abundant and were somewhat brighter than typical PNs in the Virgo galaxies (see the discussion by Feldmeier et

al. 1998). The high percentage of continuum objects (7 out of 9 detections) indicates that the off-band exposure by Feldmeier et al. was not deep enough. A re-examination of the Field 1 images by J. Feldmeier has subsequently confirmed that due to sudden changes in the seeing and transparency the off-band does go to a brighter limiting magnitude than intended. Briefly, the Field 1 exposures consisted of three 3600s on-band exposures and five 600s off-band exposures taken at the Mayall 4-m telescope. The additional off-band exposures were intended to compensate for the transparency, which was decreasing at the time of the exposures. Unfortunately, although these additional exposures do partially compensate for the change in transparency, the seeing increased by 0.3 arcsec, and consequently the mean off-band exposure is not deep enough.

On the other hand, Freeman et al. (1999) did confirm spectroscopically some fainter PN candidates in Field 1. Taken together, these results imply that the surface density of the intracluster stellar population originally estimated for Field 1 has to be reduced (Freeman et al. 2000, in preparation).

In view of the result in Field 1, we immediately pointed the VLT UT1 to the La Palma field. In this field 12 PN candidates had been found, 11 reported in Méndez et al. (1997) and one found afterwards. The distribution of the 12 PN candidates in the sky made it impossible to assign slitlets to all of them in one slitlet configuration. In our first configuration we defined 1 arc sec wide slitlets for 9 PN candidates and 2 objects suspected to be QSOs or starbursts because they were visible (although much weaker) in the off-band discovery image (Méndez et al. 1997). On the April nights 15/16 and 16/17 we completed 5 MOS exposures (40 min each) of the initial slitlet configuration, and on April 19/20 we took 3 additional MOS exposures of the La Palma Field (again 40 min each) with a different slitlet configuration, which allowed to add one PN candidate not observed before.

Thus spectra for a total of 10 PN candidates were acquired in the La Palma Field, and 7 were detected. They all show an isolated and narrow emission at wavelengths from 5007 to 5042 Å. In all cases this is the only feature visible in the spectrum. The other 3 PN candidates, which are relatively faint, were not detected. Perhaps their slitlets were slightly misplaced, although we would think the errors in the pixel transformation were too small to have any effects on the detectability. Perhaps some of these sources, if they are not PNs, have variable brightness.

Of the 2 QSO or starburst candidates, one was confirmed as a QSO at $z=3.13$, showing a typical broad-lined Ly α and C IV $\lambda 1550$. The other one appears to be a starburst because it shows one strong, isolated and narrow emission line, with faint continuum.

The success rate for emission line detection in the La Palma Field was satisfactorily high. It may be useful to give a few numbers for comparison with other searches, complementing information given in Méndez et al. (1997). The La Palma on-band image had a limiting magnitude $m_{5007} = 28.7$, equivalent to a flux of 10^{-17} erg cm $^{-2}$ s $^{-1}$. We would collect the same amount of photons through the on-band filter from a star of visual magnitude 25.5. The off-band image had a limiting magnitude 0.2 mag fainter. The search for candidates was done by blinking the on-band versus the off-band image. To compare with the selection criteria used e.g. by Steidel et al. (1999b) for their

narrow-band imaging survey, we define on-band and off-band magnitudes so that they coincide for an average star. All our emission-line candidates, being fainter or absent in the off-band image, have positive colors offband–onband. We can give only lower limits to the colors of candidates undetected in the off-band image. All tested emission-line candidates with colors above 1.0 mag have been spectroscopically confirmed. The lower limits to the colors of the 3 objects that were not detected with FORS are below 1.0 mag. Our 2 QSO or starburst candidates, detected in both images, have colors of 2.1 and 1.7 mag, respectively.

3. Analysis of the La Palma Field spectra

The CCD reductions were made using IRAF⁴ standard tasks. After bias subtraction, flat field correction and image combination to eliminate cosmic ray events, the object spectra were extracted and the sky background subtracted. Then the He-Ar-Hg comparison spectra were extracted and the object spectra were wavelength calibrated. Spectrograms of the standard stars G138-31 and G24-9 (Oke 1990) were used for the flux calibration.

We have designated the La Palma Field sources with LPF plus a number ordered according to the brightness in the discovery image. LPFnew is the latest PN candidate, found after the discovery paper (Méndez et al. 1997) was published. Object LPFs1 is the QSO, and LPFs2 is the object identified as a starburst from the start, because of its stronger continuum. F1-1 and F1-5 are objects 1 and 5 in Feldmeier's Field 1. F1-1 turns out to also have a very faint continuum, barely visible in the final processed spectrogram.

Figs. 1 to 3 show, respectively, the spectra of the QSO, the starburst with visible continuum, and one of the La Palma Field PN candidates showing no detectable continuum. All the LPF PN candidates look very similar, with only one emission line detected across the whole spectrum.

Having found no direct evidence of [O III] $\lambda 4959$, which would be expected if the detected emission line were $\lambda 5007$, we can put an upper limit to the percentage of our emission-line objects that can be PNs. After rejecting objects that show a continuum, which clearly cannot be PNs, we proceed in the following way:

- (1) shift the spectra, so that the wavelengths of the detected emission lines fall at 5007 Å.
- (2) normalize the intensities of the emission lines to the same value, e.g. 300.
- (3) add all the spectra and measure the intensity of the resulting $\lambda 4959$. If it is 50, for example, comparing to the expected value of 100 (since $\lambda 5007$ was defined to be 300) we can argue that 50% of the objects must be PNs.

⁴IRAF is distributed by the National Optical Astronomical Observatories, operated by the Association of Universities for Research in Astronomy, Inc., under contract to the National Science Foundation of the U.S.A.

The result of this test is shown in Fig. 4, where we have added the normalized spectra of the 7 PN candidates detected in the La Palma Field. The complete absence of $\lambda 4959$ indicates that, at most, one of the 7 candidates can be a PN. This conclusion is based on the noise level, not on any marginal detection of $\lambda 4959$. Besides, there is in Fig. 4 a hint of a weak continuum, not detectable in the individual spectra, which reinforces the rejection of these candidates as PNs.

4. Identification of the detected emission line as Ly α

Having rejected [O III] $\lambda 5007$, because $\lambda 4959$ is not visible in Fig. 4, we consider the alternatives:

(1) [O II] $\lambda 3727$ at $z = 0.35$ was confirmed in one case (object 5 in Field 1) but can be rejected in all other cases because we do not see H β , [O III] $\lambda\lambda 4959, 5007$ and H α at the corresponding redshifted wavelengths. This is illustrated in Figs. 5 and 6.

(2) Mg II $\lambda 2798$ at $z = 0.79$ can also be rejected for a similar reason: in this case we do not see [O II] $\lambda 3727$ at the expected redshifted wavelength, as illustrated in Fig. 7. The same argument can be applied to other lines: assuming C III $\lambda 1909$, we do not see $\lambda 2798$; and so on.

We conclude that the isolated emission line must be Ly α at $z = 3.1$. This identification is supported by the strength of the line: since we see at most a very faint continuum, the equivalent width is fairly large, typically 200 Å (observed) and 50 Å (rest frame). We have mentioned in Méndez et al. (1997) that very few starburst galaxies show, for example, [O II] $\lambda 3727$ stronger than 100 Å in equivalent width.

5. Implications for the surface density of intracluster PNs in Virgo

A reliable estimate of the surface density of intracluster PNs in Virgo will have to await a survey of a sufficiently large area on the sky, which is currently in progress. Our results to date and some preliminary conclusions are the following.

No PN candidates have been confirmed in the La Palma Field. Only 5 of the 12 candidates have a chance of remaining as PNs: 2 were not tested and 3 were tested but not detected. Since we have identified most of these candidates as Ly α emitters, it is clear that the intracluster PN sample size in the La Palma Field and the inferred surface density must be substantially smaller than we estimated.

On the other hand, the AAT+2df multi-object fiber spectroscopy has confirmed the existence of intracluster PNs in Fields 1 and 3 of Feldmeier et al. (1998). This will be reported in detail by Freeman et al. (2000, in preparation). These PNs are brighter than $m_{5007} = 27$. Freeman et al. will show that the contamination by Ly α emitters at these brighter magnitudes is not as important

as in the La Palma Field. Thus it appears that the fraction of Ly α emitters in [O III] narrow-band selected samples is magnitude-dependent, increasing towards fainter values of m_{5007} .

The lack of bright PNs in the La Palma Field implies a lower surface density than in other Virgo cluster positions, and may indicate some degree of clustering in the distribution of the diffuse intracluster population.

Our VLT+FORS observations have shown that a spectroscopic confirmation of intracluster PN candidates, involving the detection of both the $\lambda 4959$ and $\lambda 5007$ [O III] emission lines, is necessary.

6. Observed properties of the high-redshift Ly α emitters

In Table 1 we have collected some basic information about the narrow-lined sources: the measured Ly α fluxes, measured Ly α wavelengths, redshifts, and Ly α equivalent widths (W_λ in almost all cases lower limits, because the continuum is not detected). The measured wavelengths provide yet another argument favoring the interpretation of all these sources as unrelated to the Virgo cluster: they are randomly distributed across the on-band filter transmission curve, with no concentration at the Virgo cluster redshift (between 5020 and 5030 Å). See Fig. 8.

Notice that object LPF3 is brighter than measured in the discovery image. The reason is that in this case Ly α falls near the edge of the on-band filter transmission curve. LPF3 is remarkable also for the very large lower limit to its Ly α equivalent width.

The observed fluxes are between 2×10^{-17} and 2×10^{-16} erg cm $^{-2}$ s $^{-1}$. We are looking into a small redshift range, defined by the transmission of the on-band filter used at La Palma, of about $\Delta z = 0.04$. The La Palma Field covers 50 arcmin 2 . The total Ly α flux measured within our “discovery box” is 5×10^{-16} erg cm $^{-2}$ s $^{-1}$. Adopting $z = 3.13$, $H_0 = 70$ km s $^{-1}$ Mpc $^{-1}$ and $q_0 = 0.5$ we get a luminosity distance of 1.8×10^4 Mpc, which implies Ly α luminosities for our sources between 2×10^8 and 2×10^9 L \odot . The total Ly α luminosity within the sampled volume is 5×10^9 L \odot . The sampled comoving volume is 1650 Mpc 3 , which gives from 8 sources a comoving space density 5×10^{-3} Mpc $^{-3}$.

These numbers depend on our assumptions about the cosmological parameters: for a flat universe with $\Omega_0 = 0.2$, $\Omega_\Lambda = 0.8$, and the same z and H_0 as above, the luminosity distance becomes 3×10^4 Mpc, the sampled comoving volume 10^4 Mpc 3 , and the Ly α luminosities become larger by a factor 2.8.

7. Starburst models and derived quantities

What produces the narrow Ly α emission? Given rest frame equivalent widths below 200 Å, the most probable source of ionization is massive star formation (Charlot and Fall 1993). Active

Table 1. Observed and derived properties of Ly α emitters.

| object | flux ^a | $\lambda(\text{\AA})$ | z | $W(\text{\AA})^b$ | M_{stars}^c | SFR ^d | $M_{\text{s}} \& \text{SFR}^e$ |
|--------|-------------------|-----------------------|-------|-------------------|----------------------|------------------|--------------------------------|
| LPFs2 | 17 | 5011 | 3.121 | 33 | 21-420 | 7-140 | 5-10 |
| LPF1 | 7 | 5011 | 3.121 | ≥ 55 | 9-75 | 3-25 | 2-3 |
| LPF2 | 6 | 5026 | 3.133 | ≥ 32 | 7-150 | 3-50 | 2-4 |
| LPF3 | 10 | 5042 | 3.146 | ≥ 175 | 8-11 | 3-4 | – |
| LPF4 | 3 | 5007 | 3.118 | ≥ 14 | 4-270 | 1-90 | 1-5 |
| LPF6 | 2 | 5035 | 3.140 | ≥ 70 | 3-14 | 1-5 | 0.4-0.5 |
| LPF8 | 2 | 5034 | 3.140 | ≥ 37 | 3-44 | 1-15 | 0.6-1 |
| LPFnew | 2 | 5010 | 3.120 | ≥ 25 | 3-65 | 1-22 | 0.6-2 |
| F1-1 | 15 | 5021 | 3.129 | 45 | 19-200 | 6-67 | 4-6 |

^ameasured Ly α fluxes in units of 10^{-17} erg cm $^{-2}$ s $^{-1}$. Using the luminosity distance of 1.8×10^4 Mpc, this column also gives the Ly α luminosities, in units of 10^8 L \odot .

^bequivalent widths of Ly α transformed into the rest frame (the measured widths are $z + 1$ times larger).

^cPossible range of total stellar mass formed, in units of 10^6 M \odot , assuming starbursts of 3×10^6 yr duration; see section 7 and Fig. 14.

^dPossible range of star formation rates, in M \odot yr $^{-1}$, assuming starbursts; see section 7.

^ePossible range of total stellar mass formed, in units of 10^9 M \odot , assuming continuous star formation over 10^9 yr; see section 7 and Fig. 15. The same numbers also represent the corresponding star formation rates in M \odot yr $^{-1}$.

galactic nuclei (AGNs) might be an alternative, although there is no hint of C IV 1550 in our spectra, as shown in Fig. 9. We have taken massive star formation as our working hypothesis.

We have made a simple population synthesis model to explore some basic properties of the stellar population responsible for the ionization of the H II regions. Our main interest in doing this analysis is to estimate star formation rates and densities; we would like to verify if these Ly α sources correspond to the formation of massive giant galaxies or rather to the formation of smaller structures.

We adopt a standard initial mass function (IMF), $f(M) \propto M^{-2.35}$, stellar evolutionary models for low metallicity ($Z=0.001$; this choice of metallicity will be justified in next paragraph) from Schaller et al. (1992), and ionizing fluxes from NLTE model atmospheres with winds (Pauldrach et al. 1998), again for a low metallicity, in this case that of the SMC (5 times below solar).

The relation between the number of stellar Lyman continuum photons N_{LyC} and the Ly α luminosity can be obtained from a simple recombination model:

$$L(Ly\alpha) = h\nu(Ly\alpha) 0.68 X_B N_{LyC} \quad (1)$$

where 0.68 is the fraction of recombinations that yield Ly α (Case B, see e.g. Storey and Hummer 1995), and X_B is the product of the fraction of N_{LyC} really absorbed times the fraction of Ly α photons that really escape. We necessarily have $0 \leq X_B \leq 1$. Note that $X_B \sim 1$ requires both an optically thick nebula and very low dust content, because the large number of Ly α scatterings in an optically thick nebula will lead to their absorption by dust grains, if such grains are present in any significant number. This explains our choice of a low metallicity. How low is low? Since we do not know much about dust properties, we have used empirical information provided by Charlot and Fall (1993) in their Fig. 8, which shows Ly α equivalent widths as a function of oxygen abundance in nearby star-forming galaxies. In that figure we find that Ly α equivalent widths larger than 20 and 50 Å are associated respectively with oxygen abundances below 25% and 10% solar. In future work, to obtain more quantitative constraints, we intend to carry out Ly α radiative transfer calculations in the presence of dust and velocity fields as an extension of the work by Hummer and Kunasz (1980), Hummer and Storey (1992) and Neufeld (1990, 1991).

Figs. 10 and 11 show Ly α equivalent widths for single stars as a function of X_B and of the stellar T_{eff} . We need both a large X_B and many massive, hot main sequence stars in order to produce the observed Ly α equivalent widths.

We have explored two different histories of star formation in a low-metallicity stellar population: (a) a starburst, and (b) continuous star formation. These two alternatives are defined as star formation extending over a time (a) similar to $(3 \times 10^6$ years) and (b) much longer than $(10^9$ years) the duration of a main sequence OB star.

Figs. 12 and 13 show the resulting contour plots of Ly α equivalent widths as a function of

X_B and of the maximum main sequence mass in the population. In these figures, the quantities on the x axis allow different interpretations. In the case of a starburst, smaller values of M_{\max} can be interpreted to represent an increasing age of the starburst, or in other words the time elapsed since the starburst happened; as the starburst grows older, the most massive stars are removed from the main sequence. In the case of continuous star formation, the value of M_{\max} indicates at which mass the integration of the IMF was stopped. In other words, the left part of the plot shows a case in which very massive main sequence stars were not formed.

We can obtain Ly α equivalent widths > 50 Å only for $X_B > 0.5$ (continuous star formation) or $X_B > 0.3$ (starburst). This points to almost completely optically thick, extremely dust-poor nebulae. It is easy to understand why a large X_B is necessary. If it is small, many stellar ionizing photons are lost. In order to explain the observed Ly α fluxes we must add more massive stars, but these stars make a strong contribution to the continuum, and therefore the Ly α equivalent width must decrease.

It may seem surprising that we can get large Ly α equivalent widths at so low values of M_{\max} . The reason is that the Schaller et al. main sequence at low metallicity is shifted to rather high T_{eff} because of the low stellar opacity. This means that lower mass objects on the main sequence give much more ionizing flux than at solar metallicity.

The source LPF3 can be explained only as a very young starburst with $X_B \sim 1$, because of its very large Ly α equivalent width.

We set the lower mass limit of the Salpeter IMF at $0.5 M_{\odot}$. For a maximum stellar mass of $120 M_{\odot}$, this gives an average mass of $1.65 M_{\odot}$, which is then the conversion factor between number of stars and total stellar mass. The average mass decreases only slightly if we decrease M_{\max} , and only if M_{\max} is interpreted as in Fig. 13, because in that case very massive stars are not formed. The average mass does not decrease if M_{\max} is low due to the age of the starburst, because the very massive stars are assumed to have formed and evolved away from the main sequence.

Figs. 14 and 15 show contour plots of the logarithms of Ly α luminosities in a plane where the x axis is the same M_{\max} used in Figs. 12 and 13, and the y axis is the product of X_B times the total number of stars produced over the total duration of the star formation (3×10^6 and 10^9 yr, respectively). The number of stars required to produce a given Ly α luminosity depends on the value of M_{\max} . Since we cannot determine M_{\max} empirically or derive it from first principles, we have considered the full range of M_{\max} , from $120 M_{\odot}$ to as low as permitted by the limits on the Ly α equivalent widths; sometimes as low as $20 M_{\odot}$. This produces rather large uncertainties in the derived masses, particularly in the case of starbursts. A comparison of Figs. 14 and 15 also shows that, as expected, in the case of continuous star formation many more stars are needed to obtain a given Ly α luminosity.

The results of these mass estimates are listed in Table 1. The total masses of stars and star formation rates turn out to be very sensitive to the star formation history. For continuous star formation and young starbursts, i.e. high values of M_{\max} , our strongest sources have SFRs of the

order of $10 \text{ M}_\odot \text{ yr}^{-1}$. However these numbers increase dramatically if we consider older starbursts, and we cannot rule out SFRs higher than $200 \text{ M}_\odot \text{ yr}^{-1}$ in a few cases.

Adding up the masses and SFRs in Table 1, and using the average stellar mass of 1.65 M_\odot , we have built Table 2, which provides the total number and total mass of stars formed, and the resulting star formation rate, needed to explain our total Ly α luminosity of $5 \times 10^9 \text{ L}_\odot$ in the La Palma Field, for the cases of starbursts and continuous star formation. Here we have not added the numbers for F1-1, which belongs to another field.

How uncertain are these numbers? First of all, the real SFR might be higher than we inferred for our sources because of extinction by dust. However, we consider this to be unlikely because it would be necessary to argue that there is dust in the foreground (to produce extinction) but not inside (it would destroy the Ly α emission). We do not argue in terms of low metallicity because there is at least one case of a very metal-deficient blue compact dwarf galaxy, SBS 0335-052, where dust patches are clearly visible (Thuan and Izotov 1999). Note however that this source has Ly α in absorption, implying that extinction is accompanied by destruction of Ly α emission, as expected. Based on this reasoning we do not include a correction for extinction in our Tables.

The reader may argue that geometry probably plays the dominant role in dictating how many Ly α photons escape, making our attempt to estimate star formation rates a futile exercise. However, our sources are a rather special case. Geometry is useful when we need to explain why a star-forming region shows Ly α in absorption; see e.g. Kunth et al. (1998). But our sources do show strong Ly α emission, and furthermore, show a very faint continuum. The absence of continuum (i.e. the large equivalent width of Ly α) is very important because it precludes the existence of large amounts of hot stars. If there is any significant destruction of Ly α photons, then, in order to explain the observed Ly α fluxes we must add more massive stars. But these additional stars contribute to the continuum, and the Ly α equivalent width decreases too much. Thus the absence of continuum acts as a "safety valve" restricting higher values of the star formation rate. As explained above, extinction by dust is not very likely.

On the other hand, the derived masses and SFRs are strongly dependent on the lower mass limit of the IMF. If we selected a lower mass limit of 0.1 instead of 0.5 M_\odot there would be no change in the number of stars needed to produce the ionizing photons, but we would be adding a lot of low-mass stars; the total mass estimate for a given total Ly α luminosity would increase by a factor 1.9. The SFRs would have to be corrected by the same factor. The ranges of masses and SFRs in Tables 1 and 2 do not include this source of uncertainty, but we will take it into account in the discussion.

The adopted cosmological parameters also have some influence. We have adopted $H_0=70 \text{ km s}^{-1} \text{ Mpc}^{-1}$ and $q_0=0.5$, which implies a sampled comoving volume of 1650 Mpc^3 . If we take, for example, a total SFR of $50 \text{ M}_\odot \text{ yr}^{-1}$, we get a star formation density in the comoving volume of $0.03 \text{ M}_\odot \text{ yr}^{-1} \text{ Mpc}^{-3}$. If we adopted a universe with $\Omega_0=0.2$, $\Omega_\Lambda=0.8$, but with the same z and H_0 , then our star masses and SFRs would be larger by the same factor 2.8 as for the luminosities.

However the star formation density mentioned above would drop from 0.03 to 0.014 $M\odot$ yr^{-1} Mpc^{-3} because of the enlarged sampled comoving volume of 10^4 Mpc^3 .

8. Discussion

Recent blank field searches for Ly α emitters have been successful at redshifts from 2.4 to 5: Hu 1998, Cowie and Hu 1998, Pascarelle et al. 1998, Hu et al. 1998. The sources that have been verified spectroscopically (Hu 1998, Hu et al. 1998) are like ours: strong, narrow, isolated emission line identified as Ly α , with a similar range of equivalent widths.

One may ask why the earlier searches failed to detect such emission-line sources. For example Thompson et al. (1995) reported no detection in a total area of 180 arcmin 2 down to a 1- σ limiting flux 10 times fainter than the flux of our brightest source, LPFs2. This might be attributed to a very low surface or space density in their directions, but since they looked in many directions this interpretation looks improbable. The surface density in the La Palma Field does not seem to be abnormally high. The 8 sources we detected in the 50 arcmin 2 of the La Palma Field and within our redshift range of 0.04 are equivalent to 14400 emitters deg $^{-2}$ per unit z with Ly α fluxes above 1.5×10^{-17} erg cm $^{-2}$ s $^{-1}$. This is a lower limit to the true density of such sources; if some of the three photometric candidates not detected and of the two candidates not tested are Ly α emitters with similar fluxes, the true density could be higher by up to 60%. The density inferred from the present spectroscopic sample is similar to the 15000 deg $^{-2}$ per unit z reported by Hu et al. (1998) from Keck searches in different regions of the sky, with the same limiting flux. Our sources are brighter than those detected with the Keck telescope (Hu 1998, Cowie and Hu 1998, Hu et al. 1998), but our redshift is smaller; see Fig. 16. In summary, the surface density of Ly α emitters in the La Palma Field is of the same order of magnitude as for the sources detected by Hu et al. Pascarelle et al. (1998) report an order-of-magnitude range of space densities at $z = 2.4$, in some cases even higher than ours. More surveys will probably clarify whether or not there is any structure or clustering in the distribution of Ly α emitters.

Concerning masses and star formation rates, if we adopt continuous star formation or young starbursts, where star formation has not yet (or has just) stopped, then from Table 1 we read that our strongest sources show a SFR not higher than about $10 M\odot$ yr^{-1} , similar to the maximum SFRs reported by Hu et al. (1998), and short of what would be expected from a proto-giant spheroidal galaxy forming more than 10^{11} $M\odot$ in 10^9 years. We cannot completely rule out the possible existence of an inconspicuous stellar population, already formed, which would be detectable only in the infrared, but we would find it difficult to explain the very low dust content in that case. The possible existence of undetected neutral and molecular H gas would provide additional means to scatter and eventually destroy the Ly α photons (e.g. Neufeld 1990), and therefore we consider it unlikely. Thus from the available evidence we would seem to be witnessing the formation of small subgalaxies, some of which are perhaps destined to merge. This conclusion is also supported by the total mass produced, even in the case of continuous star formation, and would be unchanged if

we adopted the lowest IMF mass limit of $0.1 M_{\odot}$. If we also adopted the flat accelerating universe with $\Omega_0=0.2$ and $\Omega_{\Lambda}=0.8$, which implies larger distances, luminosities and SFRs, the starbursts would still point to small entities, but the continuous star formation in the case of LPFs2 would be able to produce several times $10^{10} M_{\odot}$.

On the other hand, continuous star formation implies the previous production of supernovae and metals, which makes it more difficult to explain a very low dust content. For that reason we consider young starbursts more likely than continuous star formation or old starbursts. But in dealing with this subject we prefer to be cautious and leave all conceivable options open.

What would happen if we allowed for older starbursts, in which star formation has stopped 10^7 years ago? Then the mass of stars formed would increase substantially, but notice that in such cases the mass produced after star formation has stopped is not larger than $10^9 M_{\odot}$. Therefore even in this extreme case starbursts are not able to make a proto-giant spheroidal galaxy out of any of our sources. This conclusion would not be weakened by assuming the accelerating universe mentioned above.

Now we try to estimate lower and upper limits for the star formation density in the sampled comoving volume that corresponds to the La Palma Field, assuming that we can rule out production of Ly α photons through AGN activity. A lower limit for the SFR of $15 M_{\odot} \text{ yr}^{-1}$ comes from the continuous star formation case in Table 2. The maximum SFR in Table 2 (old starbursts) is rather improbable, because it is obtained assuming that all the starbursts ended at the same time, some 10^7 years before the Ly α photons we detected were emitted. A more reasonable upper limit is obtained assuming that one of the starbursts is at the right age to produce the maximum SFR, while all the others make smaller contributions. Let us assume that the source produced by the only allowed old starburst is LPFs2, which would then contribute $140 M_{\odot} \text{ yr}^{-1}$. Adding the almost negligible contributions from the other sources, we obtain in this way a range of plausible total SFRs in the comoving volume between 15 and $170 M_{\odot} \text{ yr}^{-1}$. Allowing now for the uncertainty in the lower mass limit of the IMF, we get a range between 15 and $320 M_{\odot} \text{ yr}^{-1}$, which implies a star formation density between 0.009 and $0.19 M_{\odot} \text{ yr}^{-1} \text{ Mpc}^{-3}$. For comparison, Hu et al. (1998) obtained, from their own samples, 0.01 in the same units.

In order to compare our star formation density with other available information, we adopt in this paragraph $H_0=50 \text{ km s}^{-1} \text{ Mpc}^{-1}$ and $q_0=0.5$, which is what other authors have done, e.g. Steidel et al. (1999a). This gives luminosities twice as large as in our earlier choice, and a sampled comoving volume of 4500 Mpc^3 . Our resultant star formation density drops slightly to between 0.007 and $0.14 M_{\odot} \text{ yr}^{-1} \text{ Mpc}^{-3}$. This is plotted in Fig. 17 together with other data collected from several galaxy surveys by Steidel et al. (1999a). Our star formation density in Ly α emitters is comparable to that in other star forming sources at that redshift. Our sources are probably the low-metallicity (or low-dust) tail in a distribution of star forming regions at high redshifts. This is underlined by the fact that in our sampled volume we also have a QSO (LPFs1) with apparently higher metal abundances, judging from the strength of the C, N, O lines in its spectrum.

As already remarked by Hu et al. (1998), since we expect lower metallicity at higher redshifts, we should expect the strong Ly α emitters to become more frequent at higher redshifts relative to Lyman-break galaxies, which normally have weak or absent Ly α emission and are therefore presumably more metal-rich. Note, however, that low metallicity does not necessarily imply emission in Ly α : the blue compact dwarf galaxy SBS 0335-052 (Thuan and Izotov 1999), with $Z = Z_{\odot}/41$ and Ly α in absorption, provides a beautiful cautionary note. Kunth et al. (1998) have argued that the geometry and velocity structure of the interstellar medium play an important role in determining the strength of the Ly α emission, and this may complicate the comparison between Ly α emitters and Lyman-break galaxies.

Finally, we consider our Ly α emitters as possible sources of ionization of the intergalactic medium at high redshift (see e.g. Madau et al. 1998). Keeping the same cosmological parameters as in last paragraph, we get a total $L(\text{Ly}\alpha)$, in our sampled comoving volume, of $10^{10} L_{\odot}$. Converting this into N_{LyC} using Eq. (1), on the assumption that $X_B = 0.5$, we get 7×10^{54} photons s^{-1} . Since the sampled comoving volume is 4500 Mpc^3 , this implies a ionizing photon density of 1.5×10^{51} photons $\text{s}^{-1} \text{ Mpc}^{-3}$. This is the total number of ionizing photons produced by the stars. It is very difficult to estimate what fraction is available for ionization of the intergalactic medium, because it depends on the relative contributions of the two factors that enter into X_B . In at least one case (LPF3) we have $X_B \sim 1$, which means that this source cannot contribute many ionizing photons. Assuming optimistically that there remain 10^{51} ionizing photons $\text{s}^{-1} \text{ Mpc}^{-3}$ available, our Ly α emitters seem to contribute about 0.5 times as much as the star-forming galaxies at $z = 3$ found in Lyman-break galaxy surveys (see e.g. Fig. 2 of Madau et al. 1998). We conclude that the contribution by Ly α emitters may be comparable in order of magnitude to what QSOs provide at $z = 3$.

9. Summary of conclusions and perspectives

We have discovered a population of high-redshift Ly α emitters in our sample of Virgo intracluster PN candidates obtained with an “on-band/off-band” filter technique. Our VLT+FORS spectra show that the Ly α emitters at $z = 3.13$ look very similar to those discovered in other fields at other redshifts by Hu et al. (1998). Only a narrow and strong Ly α emission is visible in their spectra; no other spectral line, and no (or at most a very weak) continuum. On the assumption that Ly α emission is produced by massive star formation, we have estimated the total mass of stars formed and star formation rates, and we have estimated the star formation density in our sampled comoving volume. The Ly α emitting nebulae must be nearly optically thick and extremely dust-poor, probably indicating a very low metallicity. The total mass formed and the SFRs appear to suggest that we are witnessing the formation of rather small galaxies. This conclusion depends on several assumptions about the IMF, star formation history and cosmological parameters. There is one source (LPFs2) that might qualify as a proto-giant spheroidal if we assumed continuous star formation, a lower mass cutoff of $0.1 M_{\odot}$ in the IMF, and a flat accelerating universe with $\Omega_0=0.2$

and $\Omega_\Lambda=0.8$. However, to assume continuous star formation implies the previous production of supernovae and metals, making it more difficult to explain the very low dust content required by the observed spectra of our sources. We are more probably dealing with young starbursts.

Taking all sources into account, the implied star formation density in our sampled comoving volume is probably somewhat smaller than, but of the same order of magnitude as the star formation density at $z \sim 3$ derived by other authors from Lyman-break galaxy surveys. This result agrees with the expectation that the Ly α emitters are a low-metallicity (or low-dust) tail in a distribution of star forming regions at high redshifts. Finally, the Ly α emitters may contribute as many H-ionizing photons as QSOs at $z \sim 3$. They are therefore potentially significant for the ionization budget of the early universe.

More extensive surveys at different redshifts will be needed to build a luminosity function for the Ly α emitters and to decide if they show any evidence of clustering and evolution as a function of redshift. HST images might be able to resolve these sources; their morphology might offer clues about their star formation processes. High-resolution spectroscopy of Ly α would provide important kinematic information about the interstellar medium in these galaxies. We need infrared spectra to try to detect forbidden lines and either determine or put some upper limits to the metallicity. It might also be possible to clarify to what extent the production of Ly α photons can be attributed to AGN activity. The firm detection of an infrared continuum would help to constrain the characteristics and total mass of the stellar populations through comparison with population synthesis models.

The implications of our results for the surface density of the diffuse intracluster stellar population in the Virgo cluster are not clear yet. Future searches for intracluster PNs will have to include the spectroscopic confirmation of the candidates, by detection of the two bright [O III] emissions at 4959 and 5007 Å. From the spectroscopic work of our group to date, including the confirmation of 23 intracluster PNs by the detection of the two [OIII] lines by Freeman et al. (1999), the fraction of high-redshift Ly α sources in the on-band/off-band samples appears to be higher at faint magnitudes. In the specific case of the “La Palma Field” we have not found any intracluster PNs, perhaps suggesting some degree of clumpiness in the distribution of the intracluster stellar population. In other Virgo fields with brighter PN candidates, the fraction of high-redshift Ly α emitters among the detected sources appears to be about 25% (see Freeman et al. 2000, in preparation, for a more extensive discussion).

RPK would like to thank the director and staff of Steward Observatory, Tucson, for their hospitality and support during an inspiring sabbatical which among other results has led to the ESO proposal 63.N-0530. Thanks also to Stefan Wagner for helpful comments. RPK and RHM express their gratitude to the ESO staff at Cerro Paranal, who contributed with their efforts to make this VLT run an enjoyable experience.

REFERENCES

Arnaboldi M., Freeman K.C., Méndez R.H. et al. 1996, *ApJ*, 472, 145

Charlot S., Fall S.M. 1993, *ApJ*, 415, 580

Cowie L.L., Hu E.M. 1998, *AJ*, 115, 1319

Feldmeier J.J., Ciardullo R., Jacoby G.H. 1998, *ApJ*, 503, 109

Ferguson H.C., Tanvir N.R., von Hippel T. 1998, *Nature*, 391, 461

Freeman K.C. et al., 1999, in *Galaxy Dynamics: from the Early Universe to the Present*, ASP Conf. Ser. , eds. F. Combes, G.A. Mamon, V. Charmandaris, in press, astro-ph/9910057

Hu E.M. 1998, *ASP Conf Ser*, 146, p. 148

Hu E.M., Cowie L.L., McMahon R.G. 1998, *ApJ*, 502, L99

Hu E.M., McMahon R.G. 1996, *Nature*, 382, 231

Hummer D.G., Kunasz P.B. 1980, *ApJ*, 236, 609

Hummer D.G., Storey P.J. 1992, *MNRAS*, 254, 277

Jacoby G.H., Branch D., Ciardullo R. et al. 1992, *PASP*, 104, 599

Jacoby G.H., Ciardullo R., Ford H.C. 1990, *ApJ*, 356, 332

Kunth D., Mas-Hesse J.M., Terlevich E. et al. 1998, *A&A*, 334, 11

Madau P., Haardt F., Rees M.J. 1998, preprint astro-ph/9809058 (4 Sep 1998)

Méndez R.H., Guerrero M.A., Freeman K.C. et al. 1997, *ApJ*, 491, L23

Neufeld D.A., 1990, *ApJ*, 350, 216

Neufeld D.A., 1991, *ApJ*, 370, L85

Oke J.B. 1990, *AJ*, 99, 1621

Pascarelle S.M., Windhorst R.A., Keel W.C. 1998, *AJ*, 116, 2659

Pauldrach A.W.A., Lennon M., Hoffmann T.L. et al. 1998, *ASP Conf Ser*, 131, p. 258

Schaller G., Schaerer D., Meynet G., Maeder A. 1992, *A&AS*, 96, 269

Steidel C.C., Adelberger K.L., Giavalisco M. et al. 1999a, preprint astro-ph/9811399v2 (23 Jan 1999)

Steidel C.C., Adelberger K.L., Shapley A.E. et al. 1999b, preprint astro-ph/9910144 (7 Oct 1999)

Storey P.J., Hummer D.G. 1995, MNRAS, 272, 41

Thompson D., Djorgovski S., Trauger J. 1995, AJ, 110, 963

Thuan T.X., Izotov Y.I. 1999, preprint astro-ph/9902369 (25 Feb 1999)

Fig. 1.— The spectrum of QSO candidate LPFs1. The strong, broad emissions ($\text{Ly}\alpha + \text{N V } \lambda 1240$ and $\text{C IV } \lambda 1550$) confirm that this is a QSO at a redshift $z = 3.13$ (the observed wavelength of $\text{Ly}\alpha$ is 5024 Å). A faint continuum is visible only longward of 3760 Å, which is consistent with the position of the Lyman break. Other features visible are $\text{O VI } \lambda 1035$ at 4275 Å, $\text{O IV} + \text{Si IV } \lambda 1402$ at 5790 Å, and $\text{He II } \lambda 1640$ at 6775 Å.

Fig. 2.— The isolated emission in the spectrum of starburst candidate LPFs2. A continuum is clearly seen, as expected from the off-band detection in the discovery paper.

Fig. 3.— The isolated emission in the spectrum of PN candidate LPF3. Here no continuum is detected, consistent with the off-band non-detection in the discovery paper.

Fig. 4.— Addition of the normalized spectra of 7 PN candidates (no individual continua detected). The normalization procedure is described in section 3. The arrow indicates where $[\text{O III}] \lambda 4959$ should be, if the visible emission were $[\text{O III}] \lambda 5007$. The absence of 4959 leads to conclude that probably none, and at most one, of the 7 candidates can be a PN. Note also that in this added spectrum a very faint continuum may be visible.

Fig. 5.— The upper spectrum corresponds to an anonymous galaxy in the La Palma Field which happened to show strong emission at $[\text{O II}] \lambda 3727$, $\text{H}\beta$ and $[\text{O III}] \lambda\lambda 4959, 5007$. We use this object as reference; its continuum has been arbitrarily rectified for easier comparison. Below this star-forming galaxy we show the spectrum of F1-5 (object 5 in Field 1), redshift-corrected so that the strong emission line detected with the on-band filter falls at 3727 Å. F1-5 shows the same set of starburst emission lines as the reference galaxy, and therefore its redshift is confirmed to be 0.35. Below we have plotted the spectra of our sources, all redshift-corrected in the same way as for F1-5. The levels of zero intensity are separated by 500 counts. None of these sources shows other emission lines at the relevant wavelengths.

Fig. 6.— The upper spectrum corresponds to another anonymous galaxy, this time in Field 1, which shows emission at $\lambda 3727$, $\lambda 5007$ and $\text{H}\alpha$. The arrow indicates the position of $\text{H}\alpha$. Below it, from top to bottom, we show the spectra of 6 of our sources, all redshift-corrected as described in Fig.5. The levels of zero intensity are separated by 500 counts. None of these sources shows any convincing evidence of emission at the expected wavelength of $\text{H}\alpha$. The “inverted P Cyg features” in the spectra of LPFs2 and LPF1 are artifacts produced by imperfect sky subtraction in the presence of very strong sky emission lines. We have verified by careful inspection of the combined CCD spectrograms that no real features are visible at those wavelengths. The spectra of the sources which are not shown here do not reach so large wavelengths, because of their positions in their respective fields. This figure and the previous one show that we cannot attribute the detected emission lines to $[\text{O II}] \lambda 3727$.

Fig. 7.— Here all spectra have been redshift-corrected so that the strong emission line detected with the on-band filter falls at $\text{Mg II } 2798$ Å. The levels of zero intensity are separated by 500 counts. Nothing is visible at the expected position of $[\text{O II}] \lambda 3727$, indicated with an arrow.

Fig. 8.— The full line is the transmission curve of the on-band filter used at La Palma. The histogram shows the wavelength distribution of the emission lines. One object corresponds to 1 unit along the y axis. Our sources are more or less uniformly distributed across the filter curve.

Fig. 9.— Spectra of our sources in the rest frame of Ly α . At the top is the QSO LPFs1. The levels of zero intensity are separated by 500 counts. Only the QSO shows C IV λ 1550. At some wavelengths a slightly larger noise level is noticeable; this is due to imperfect sky subtraction in the presence of very strong sky emission lines. In several cases where the disturbance by the sky lines was too bad, we have replaced the spectrum by a straight line at zero intensity.

Fig. 10.— Equivalent width of Ly α emission produced by a single star, as a function of the stellar T_{eff} , calculated for $X_B = 0.3$.

Fig. 11.— Equivalent width of Ly α emission produced by a single star, in the plane T_{eff} vs. X_B . The contour lines are labeled with the Ly α equivalent widths in Å.

Fig. 12.— Contour plots of Ly α equivalent widths in Å, as a function of X_B and M_{max} (the maximum main sequence mass in the population), for the case of a starburst. See text.

Fig. 13.— Same as Fig. 12, for the case of continuous star formation. See text.

Fig. 14.— Contour plots of the logarithms of Ly α luminosities, in units of L_{\odot} , for the case of a starburst. Given a Ly α luminosity, it is possible to read, for different values of M_{max} , the product of X_B times the total number of stars.

Fig. 15.— Same as Fig. 14, for the case of continuous star formation.

Fig. 16.— The logarithms of observed Ly α fluxes (in $\text{erg cm}^{-2} \text{s}^{-1}$) as a function of redshift. The plus signs are our sources, and the vertical bars represent the ranges of fluxes observed by Hu (1998) at redshifts 3.4 and 4.6. The dashed lines represent the observed fluxes for Ly α luminosities of 10^{42} and 10^{43} erg s^{-1} , if we assume $H_0=70 \text{ km s}^{-1} \text{ Mpc}^{-1}$ and $q_0=0.5$.

Fig. 17.— Logarithms of star formation density in $M_{\odot} \text{ yr}^{-1} \text{ Mpc}^{-3}$, as a function of redshift. The lines show the results derived from galaxy surveys, collected by Steidel et al. (1999a): neglecting (dashed) and correcting for (solid) extinction by dust. These curves are derived assuming continuous star formation. Our star formation densities at $z = 3.13$ have been adapted, for consistency, to the same cosmological parameters used by Steidel et al. The square and diamond represent, respectively, our results assuming continuous star formation and starbursts. Both symbols have been slightly displaced horizontally for legibility.

Table 2. Star formation needed to explain the total Ly α luminosity in the La Palma Field.

| star formation | $N_{\text{stars}}^{\text{a}}$ | total $M_{\text{stars}}^{\text{b}}$ | SFR $^{\text{c}}$ |
|----------------|-------------------------------|-------------------------------------|-------------------|
| starburst | $4-65 \times 10^7$ | $6-105 \times 10^7$ | 19-350 |
| continuous | $7-15 \times 10^9$ | $12-26 \times 10^9$ | 15-30 |

^aTotal number of stars formed

^bTotal mass of stars formed, in M_{\odot}

^cStar formation rate in $M_{\odot} \text{ yr}^{-1}$

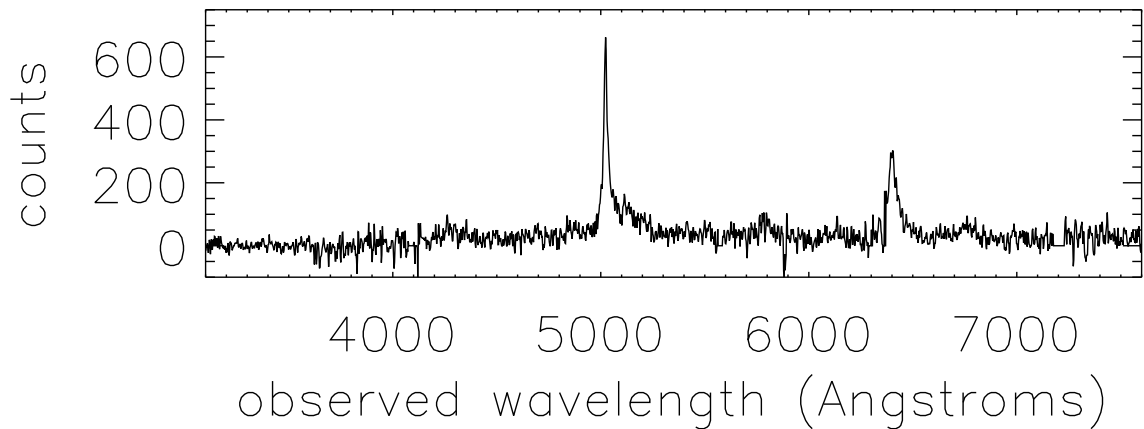


Fig. 1.— Figure 1

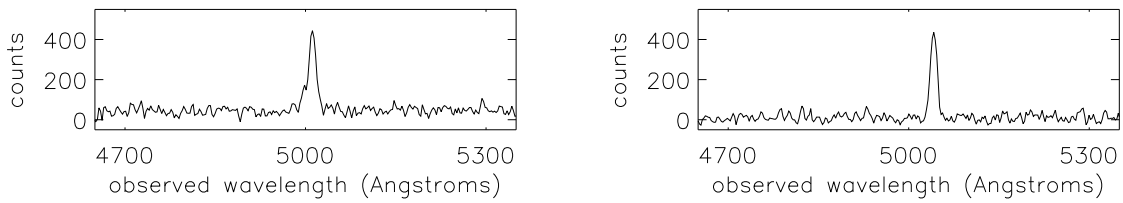


Fig. 2 and 3.— Figures 2 and 3

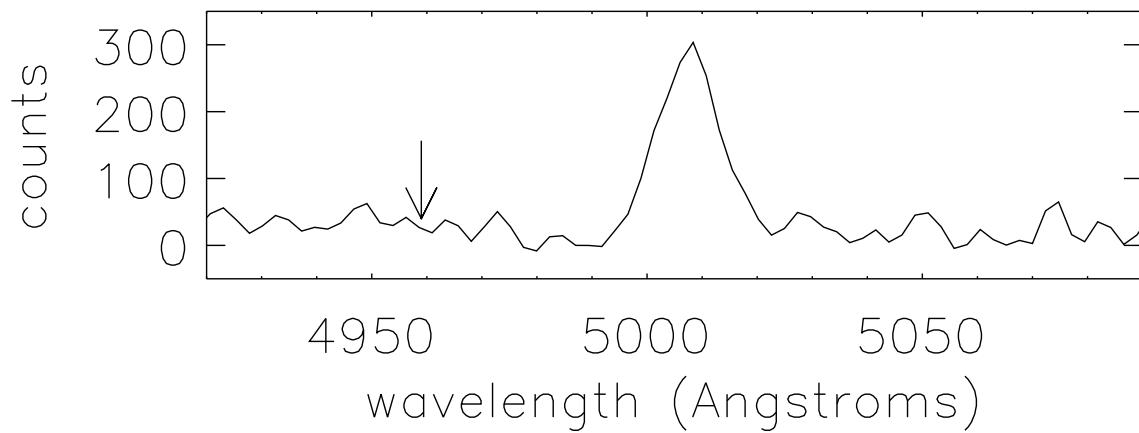


Fig. 4.— Figure 4

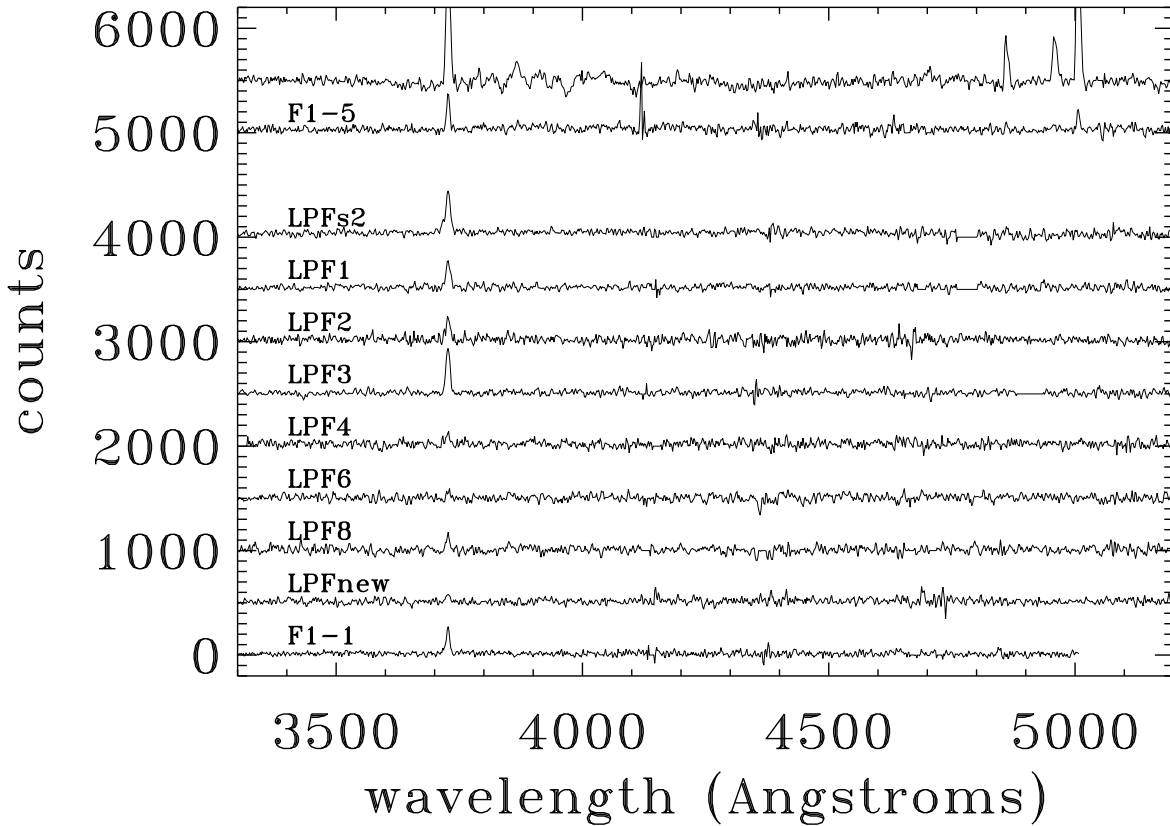


Fig. 5.— Figure 5

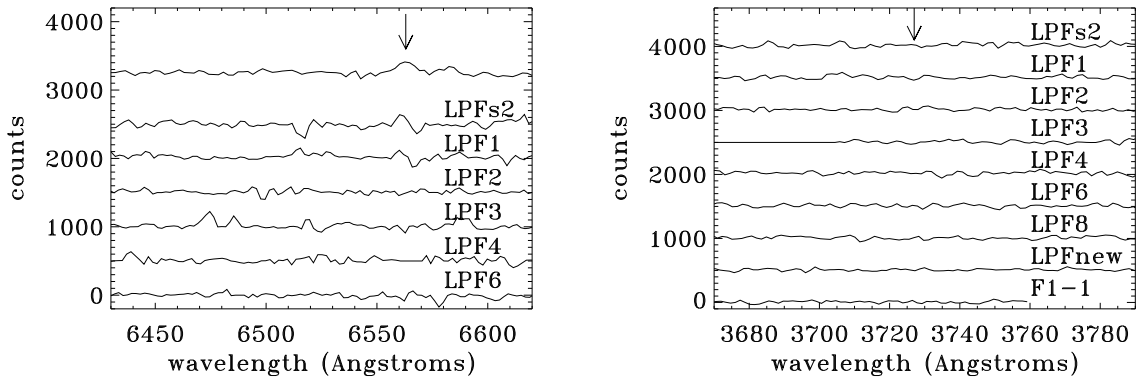


Fig. 6 and 7.— Figures 6 and 7

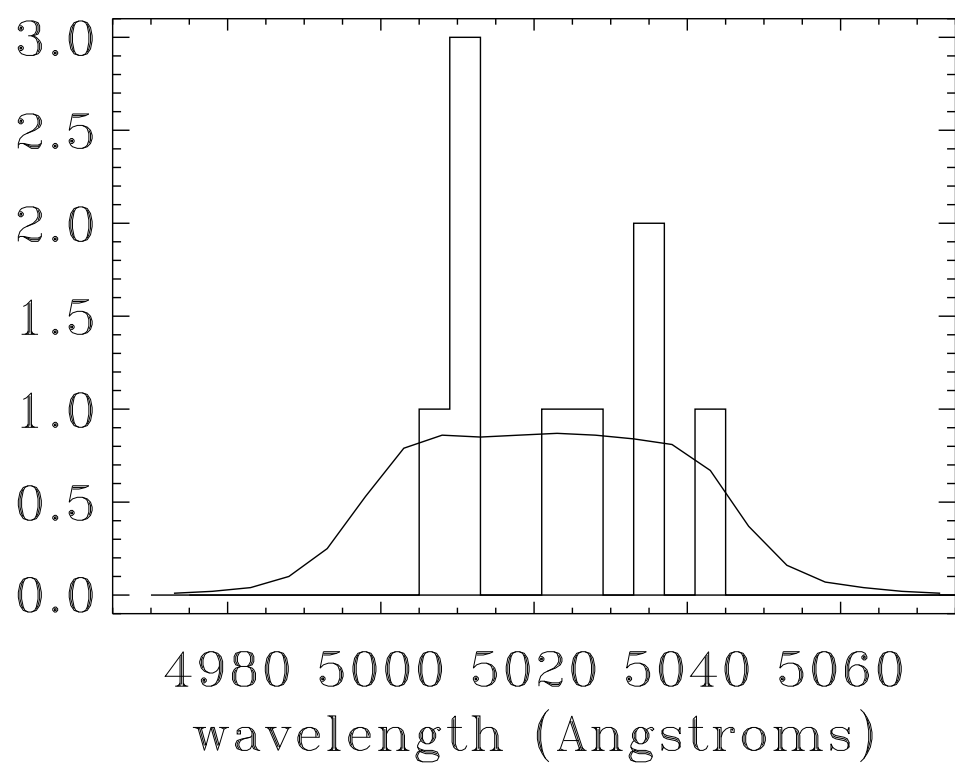


Fig. 8.— Figure 8

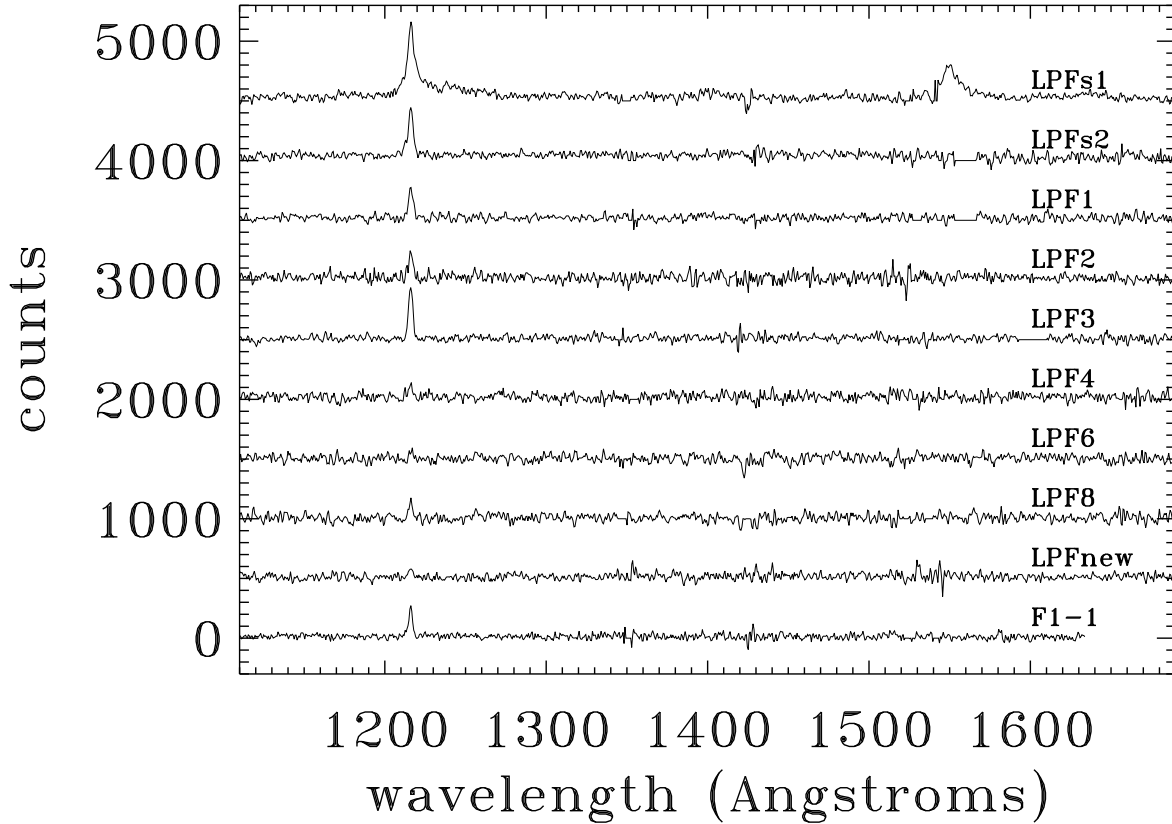


Fig. 9.— Figure 9

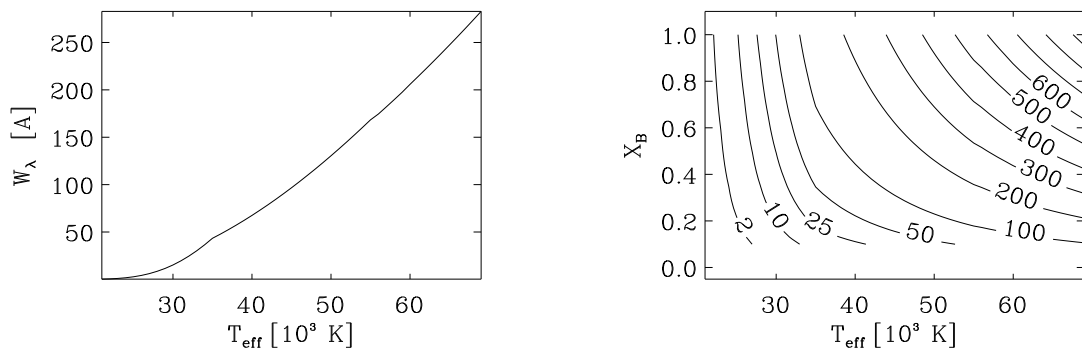


Fig. 10 and 11.— Figures 10 and 11

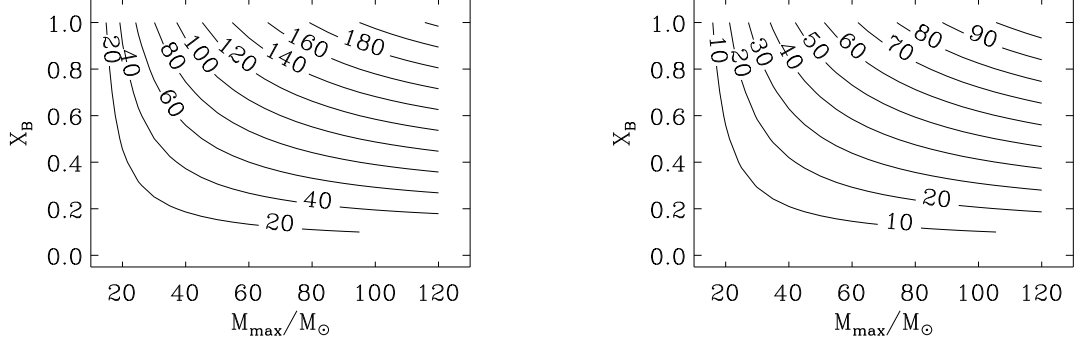


Fig. 12 and 13.— Figures 12 (starburst) and 13 (continuous star formation)

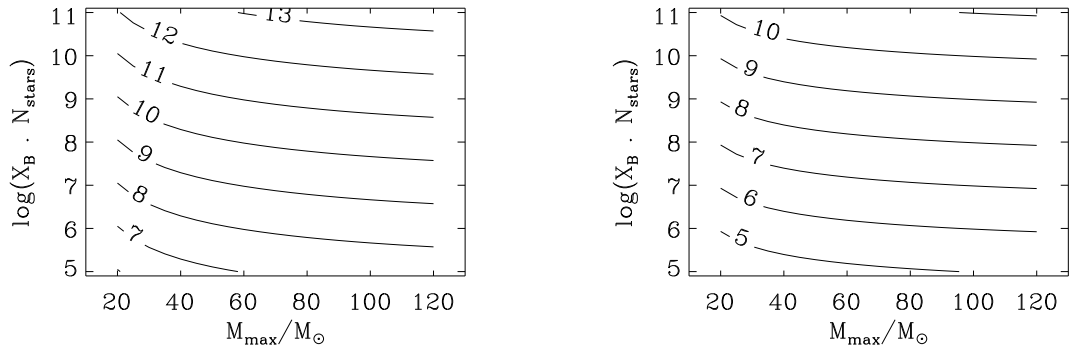


Fig. 14 and 15.— Figures 14 (starburst) and 15 (continuous star formation)

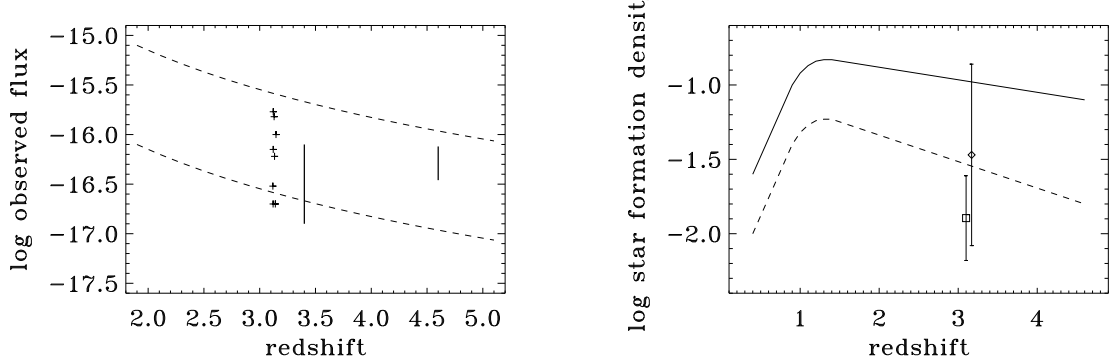


Fig. 16 and 17.— Figures 16 and 17